Role of Crack Tip Shielding Mechanisms in Fatigue of Hybrid Epoxy Composites Containing Rubber and Solid Glass Spheres

H. R. AZIMI, R. A. PEARSON,* and R. W. HERTZBERG

Department of Materials Science and Engineering and Center for Polymer Interfaces, Lehigh University, Bethlehem, Pennsylvania 18015

SYNOPSIS

The fatigue crack propagation (FCP) resistance of epoxy-based composites containing various concentrations of solid glass spheres (SGS) and/or reactive liquid rubber (CTBN) was examined. The FCP results show that the simultaneous use of rubber and solid glass spheres (hybrid composites) results in synergistic improvement in FCP resistance of composites through the entire crack growth regime. The nature of synergistic interactions was elucidated by careful examination of the fatigue fracture surfaces and the subfatigue fracture surfaces of fatigue samples. It was shown that when rubber particles cavitate in the vicinity of the glass spheres, regardless of the nature of the interface, glass particle debonding from the matrix is suppressed due to a change in the crack tip localized stress state. This, in turn, results in improved pinning/bridging efficiency of the glass spheres. Furthermore, it was shown that crack tip plastic zone–rubber particle interactions induce a transition in FCP behavior of rubber-modified epoxies. Consequently, crack tip shielding mechanisms become active when the size of the plastic zone at the crack tip becomes large compared to the size of the rubber particles. © 1995 John Wiley & Sons, Inc.

INTRODUCTION

Two common approaches taken to improve the crack propagation resistance of otherwise brittle epoxy polymers include (1) modification of the epoxy matrix using compliant rubbery particles[1-3] and (2) reinforcement of the epoxy matrix using rigid inorganic fillers.[4,5] The addition of a compliant rubbery phase can toughen the epoxy polymers by promoting process zone mechanisms such as cavitation/shear banding and plastic void growth.[2,6-8] Shear banding and plastic void growth mechanisms reduce the effective crack driving force by forming a plastic zone at the crack tip, thereby shielding the crack tip from the applied crack driving force. Generally, for a given system, such mechanisms result in a toughness that typically scales with the size of the plastic zone.[8-10]

On the other hand, the addition of glass fillers toughens epoxy polymers through crack tip pinning/crack surface bridging mechanisms.[4,5,11-13] Pinning the crack tip causes the crack front to bow between the rigid impenetrable particles, thereby absorbing more energy due to line tension effects.[11] In addition to the line tension effects, the rigid particles bridge the two crack surfaces; the latter provides resistance to crack opening by applying closure forces which directly reduce the crack driving force at the crack tip. Theoretically, pinning/bridging mechanisms result in a toughness which scales with the size of the bridging zone.[14]

More recently, a third approach has been employed which involves the development of hybrid epoxy composites.[15-17] Hybrid epoxy composites are epoxy polymers modified with both rubbery particles and rigid fillers. The objective of developing this type of composite is to promote the simultaneous occurrence of cavitation/shear banding induced by rubber particles and crack tip pinning/crack surface bridg-

* To whom correspondence should be addressed.

Journal of Applied Polymer Science, Vol. 58, 449–463 (1995)
 CCC 0021-8995/95/020449-15

ing mechanisms induced by rigid glass spheres. Ideally, these toughening mechanisms should interact in a positive manner so that for a given volume fraction of modifiers, the toughness of the hybrid composite would be greater than the toughness of the composite modified by either of the modifiers. Such positive interactions have been predicted theoretically[8,18] and observed experimentally[15-17] for static fracture toughness testings measurements.

A rubber-toughening model by Evans et al.[8] indicates that the interaction of the bridging mechanism with the cavitation/shear yielding and plastic void growth mechanisms should result in synergistic toughening. The issue of synergistic toughening in a shear yielding epoxy polymer modified by both small (1–2 μm) and large (100–200 μm) rubber particles has been investigated by Pearson and Yee.[9] The small rubber particles would be expected to interact with the crack tip plastic zone, thus promoting the process zone mechanisms; alternatively, the large particles would remain intact in the plastic zone and serve to bridge the crack surfaces. Their investigation provided evidence for interactions in the system but did not show any evidence for synergistic toughening. The absence of synergistic toughening was attributed to the poor bridging efficiency of the large rubber particles. It was, therefore, concluded that the use of stiffer particles would enhance bridging efficiency and thus should lead to synergistic toughening.

Indeed, positive interactions between glass particles and rubber particles in a hybrid epoxy composite have been reported by Kinloch and his coworkers.[15] Fracture toughness values as high as 3 MPa $m^{0.5}$ were attributed to cavitation/matrix shear banding induced by rubber particles and crack tip pinning induced by glass particles. Interestingly, when the glass particles were silane-treated to increase the adhesion between the epoxy matrix and the glass particles, the fracture toughness was increased even further. This increase in fracture toughness was attributed to stronger pinning efficiency of the coated glass particles. Recently, Low et al.[16] reported synergistic toughening in hybrid epoxy composites containing small rubber particles and aligned glassy metal ribbons and short alumina fibers which are more efficient bridging elements as compared with rigid glass particles. Fracture toughness values as high as 4.2 MPa $m^{0.5}$ were reported. The authors attributed the synergistic toughening to the interactions between rubber particle cavitation/matrix plastic deformation, and ribbon debonding, breakage, pull-out, and bridging mechanisms. More recently, Smith et al.[17] reported synergistic toughening in a new type of hybrid epoxy composite—epoxy polymer modified by rubber particles and hollow glass spheres. The authors attributed the synergistic toughening to the multiplicative interactions between rubber particle cavitation/matrix shear yielding mechanisms and hollow-glass-sphere-induced microcracking as opposed to pinning or bridging mechanisms. The question posed in this investigation is whether such interactions operate under cyclic loading conditions.

Increasing interest in epoxy-based composites for structural components exposed to cyclic loads necessitates the understanding of damage accumulation and associated fracture mechanisms. However, in contrast to the case of monotonic loading, such understanding is almost nonexistent particularly as it relates to the nature of the crack tip shielding mechanisms in hybrid epoxy composites under cyclic loading conditions. Yet, it has been shown that the failure micromechanisms and fracture surfaces generated by stable fatigue crack propagation (FCP), even in a tension–tension mode, may reveal significantly different features from those under monotonic loading conditions.[19] Furthermore, the few investigations on fatigue of toughened epoxy polymers[20-23] were focused mainly on the macroscopic FCP behavior in the relatively high crack growth rate regime and did not address the determination of crack tip shielding mechanisms. Obviously, developing a better understanding of the FCP behavior of hybrid epoxy composites requires that one elucidates the role of various toughening mechanisms and the interactions among them at both low and high crack growth rates.

The objective of the present work is, therefore, to study the macroscopic FCP behavior and crack tip shielding micromechanisms for a system of hybrid epoxy composites at both low and high crack growth rate regimes. The specific questions posed in this investigation are (1) whether synergistic interactions operate under cyclic loading conditions; (2) determination of the nature of such interactions; and (3) how such interactions are affected by the interface properties between the glass particles and the epoxy matrix.

EXPERIMENTAL

Materials

The epoxy matrix used is a solid diglycidyl ether of bisphenol A epoxy resin designated as DGEBA with

Table I Formulations of the CTBN Rubber (R) and/or Solid Glass Sphere (SGS) Modified Epoxies Studied

Designation	DGEBA (g)	Piperidine (g)	CTBN-8 (g)	SGS (g)
Neat	500	11	—	—
R(10)[a]	500	11	50.0	—
TSGS(10)	500	11	—	115
SGS(10)	500	11	—	115
R(2.5)TSGS(7.5)	500	11	12.5	84.5
R(5)TSGS(5)	500	11	25.0	53.6
R(7.5)TSGS(2.5)	500	11	37.5	26.7
R(7.5)SGS(2.5)	500	11	37.5	26.7

[a] Numbers in parenthesis denotes the volume fraction of the modifier. TSGS, SGS, and R stand for treated solid glass spheres, nontreated solid glass spheres, and CTBN rubber, respectively.

an equivalent weight range of 500–560 g/mol (DER 661 resin from Dow Chemical Co.). Epoxy composites were prepared by incorporation of varying concentrations of solid glass spheres (SGS) and/or reactive liquid rubber. The SGSs were provided by Potters Industries Inc. (Spheriglass 2900). Two types of SGSs were used: one which had a silane-based coupling agent, designated CL2900-CP-03, to promote adhesion between the glass particles and the DGEBA epoxy matrix; and the other which received no surface treatment, designated CL2900. According to the supplier, these particles have an average size of 49 μm. The rubber used was a Hycar CTBN 1300 X8 reactive liquid rubber provided by B. F. Goodrich Company. The CTBN rubber is a reactive oligomer composed of carboxylic acid capped copolymer of butadiene acrylonitrile. The formulations of the composites made for this study are given in Table I.

Plaques of the hybrid epoxy composites were prepared using the following procedure. First, 500 g of the DGEBA epoxy resin were melted at 80°C and degassed with agitation. Next, rigid modifiers were added to the epoxy resin and the mixture degassed while being stirred with a high shear rate to ensure a good distribution of the modifiers. The CTBN rubber was then added to the mixture and once again the mixture was degassed with agitation before adding 11 mL of the curing agent, piperidine, which was added to the epoxy–modifiers mixture at ambient pressure with slow agitation. The curing agent–epoxy resin mixture was degassed again with agitation till the viscosity of the epoxy resin mixture was high enough to prevent sedimentation of the inorganic modifiers. The epoxy resin mixture was then poured into a 160°C preheated Teflon-coated aluminum mold. The mold was then placed in a circulating air oven to cure for 16 h at 160°C.

Tensile Testing

Tensile tests were performed on type I specimens (ASTM D638 Standard) at a crosshead speed of 10 mm/min, using a screw-driven Instron testing machine. The reported tensile test data (Table II) represent averages of three tests. A type D 1-inch gauge

Table II Tensile and Fracture Toughness Data for the Materials Studied

Compositions	E (GPa)	σ_{ys} (MPa)	K_{IC} (MPa $m^{0.5}$)
Neat	2.94 ± 0.19	71.2 ± 1	0.90 ± 0.02
R(10)	2.53 ± 0.19	56.6 ± 0.5	3.20 ± 0.04
TSGS(10)	3.60 ± 0.10	75.6 ± 0.5	1.97 ± 0.09
R(2.5)TSGS(7.5)	3.46 ± 0.19	73.2 ± 0.2	2.31 ± 0.07
R(5.0)TSGS(5.0)	3.18 ± 0.08	68.1 ± 1.4	2.77 ± 0.06
R(7.5)TSGS(2.5)	3.09 ± 0.02	63.6 ± 0.9	3.57 ± 0.06
R(7.5)SGS[†](2.5)	2.80 ± 0.15	64.5 ± 0.1	3.54 ± 0.09

extensometer was used to determine the nominal strain which allowed for the calculation of the elastic tensile modulus of the materials.

Fracture Toughness Measurements

Fracture toughness measurements were performed on precracked, single-edge notched (SEN) specimens in three-point bend geometry and in accordance with the ASTM D5045 Standard. Precracking was performed by taping a cold razor blade (immersed in liquid nitrogen) into the machined notch provided in the specimens. Tests were conducted on a screw-driven Instron 1011 materials testing machine with a crosshead speed of 2 mm/min. The fracture toughness values (Table II) represent averages of 5–8 tests and were obtained under plane strain condition.

Fatigue Crack Propagation

Fatigue crack propagation (FCP) studies were performed using notched compact tension [C(T)] specimens and in general accordance with the ASTM E647-93 Standard recommended practice. Specimens were cyclicly loaded at ambient conditions. A computer-controlled servohydraulic materials testing machine (Instron) was used to apply a sinusoidal load frequency of 10 Hz with a load ratio (R = minimum load/maximum load or $R = K_{min}/K_{max}$) of 0.1.

Crack growth data were obtained by interfacing the Instron machine to a desktop computer and using software and hardware developed by Fracture Technology Associates, Inc. Online crack length monitoring was performed via measurement of the instantaneous compliance of the specimen with a crack opening displacement (COD) gauge that was attached to knife edges located in the mouth of the notch of the C(T) specimens. Crack growth rates (da/dN) were determined from compliance-inferred crack length measurements and associated number of cycles (N), using a modified secant formulation:

$$\left(\frac{da}{dN}\right)_n = \frac{a_{n+1} - a_{n-1}}{N_{n+1} - N_{n-1}} \quad (1)$$

where a is crack length, n is iteration number, and N is number of cycles.

In order to avoid any load interaction, precracking of $C(T)$ specimens was performed under constant load conditions such that the final K_{max} of the precracking procedure was less than the initial K_{max} of the decreasing ΔK portion of the test.

The crack growth data were first generated under decreasing ΔK conditions (Fig. 1)[24] using an automated load-shedding scheme where

$$\Delta K = \Delta K_0 \exp[C^*(a - a_0)] \quad (2)$$

where ΔK is instantaneous value of stress intensity factor range ($K_{max} - K_{min}$), a is instantaneous value of crack length, ΔK_0 is initial value of stress intensity range, a_0 is initial value of crack length, and C^* is normalized stress intensity gradient $[(dK/da)/K]$ and by setting C^* to -0.08/mm of crack extension. After reaching a crack growth rate of about 10^{-6} mm/cycle, tests were continued under increasing ΔK conditions (Fig. 1)[24] by setting C^* to $+0.08$/mm. Crack growth data were plotted against ΔK, the range in the applied stress intensity factor. Stress intensities were calculated by the software and from standard stress intensity factor solutions for the compact geometry (ASTM Standard E-399).

Scanning Electron Microscopy

A JEOL 6300F low-voltage, scanning electron microscope (SEM) was used to examine the fatigue fracture surfaces of the materials tested. All fracture surfaces were coated prior to fractographic examination. A thin layer of gold-palladium, sputtered on the fatigue fracture surface, reduced the amount of the charge buildup. SEM micrographs were obtained under conventional secondary electron imaging conditions and with an accelerating voltage of 5 kV.

Optical Microscopy

An optical microscopy (OM) technique was employed to examine the nature of subsurface fatigue damage in the crack wake and at the crack tip of

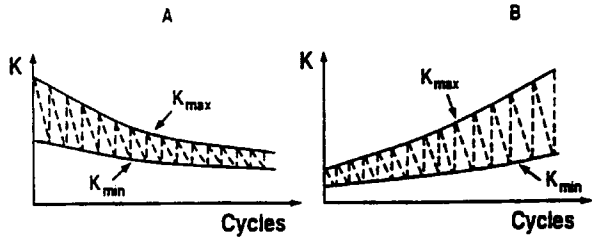

Figure 1 Schematic drawing representing R-constant decreasing ΔK (left) and R-constant increasing ΔK (right) test methodologies used in the present work.[24]

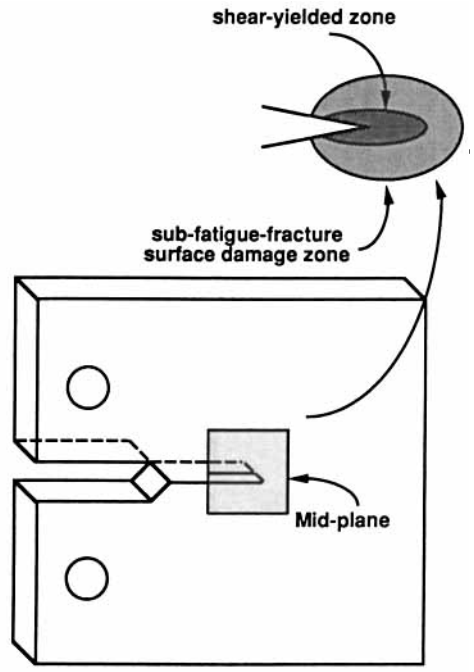

Figure 2 Schematic drawing showing the position from where the OM samples were obtained.[25]

the compact tension specimens. For this purpose, thin sections in the range of 150–200 and 30–50 μm from the crack regions (plane strain sections, see Fig. 2)[25] were prepared using petrographic polishing techniques.[19] The thin sections were viewed using a Zeiss optical microscope. The thin sections were illuminated with transmitted light. Both bright-field and crossed-polarized viewing conditions were used.

RESULTS AND DISCUSSION

Fracture Toughness

Fracture toughness data for the system studied are plotted in Figure 3. These results suggest that for a combined 10% volume fraction of modifiers, the addition of glass particles to a rubber-modified epoxy matrix results in superior toughness when compared to epoxy modified by either modifiers. This suggests that a positive interaction occurs among the mechanisms of toughening which results in synergistic behavior in the R(7.5)TSGS(2.5) hybrid composite. Similar synergism has been reported previously by several investigators for static fracture toughness testing in hybrid epoxy composites.[15–17] Kinloch et al.[15] attributed this to additional shear deformation, induced by solid glass spheres when rubber particles are present in the matrix. The occurrence of synergistic toughening for certain compositions and the lack of such behavior for others in the hybrid systems studied here can be discussed in detail for the case of static fracture behavior. However, this study focuses attention on FCP behavior and micromechanical deformation mechanisms under cyclic loading conditions.

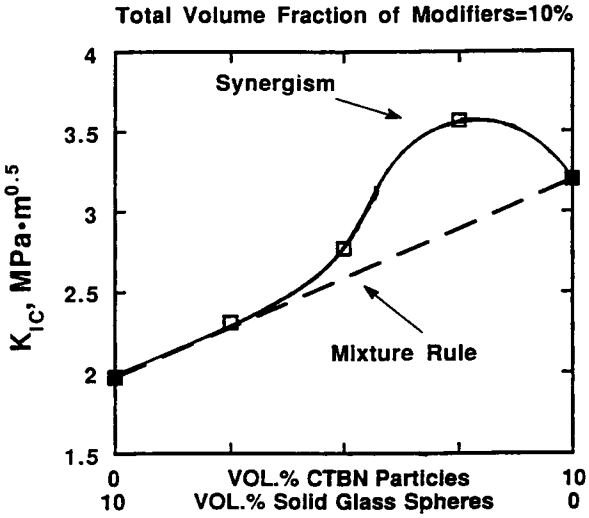

Figure 3 K_{IC} vs. the modifier content for the R/TSGS system. Note the synergistic toughening for R(7.5) TSGS(2.5) hybrid composite.

Fatigue Crack Propagation Behavior

The fatigue crack growth rates (da/dN) versus the range in the stress intensity factor (ΔK) for neat epoxy and epoxies modified by rubber and/or treated solid glass spheres are presented in Figure 4. Note that rubber toughening of the epoxy is more effective

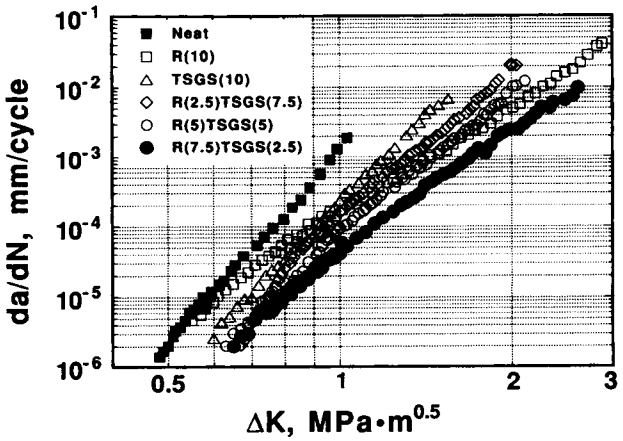

Figure 4 FCP data for the R/TSGS composites.

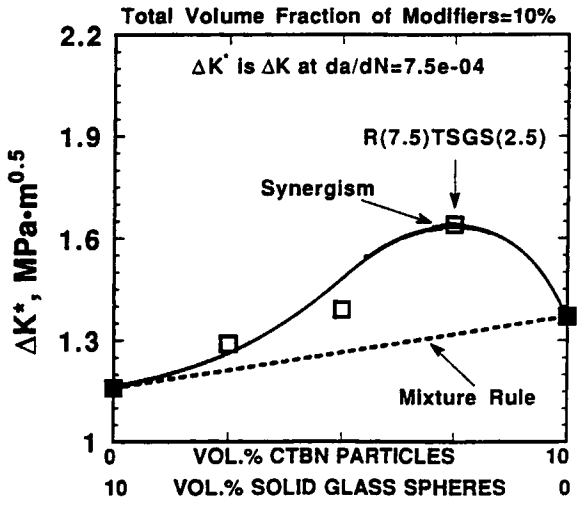

Figure 5 Synergistic behavior observed in FCP experiments of R/TSGS hybrid system. Note that the hybrid composite R(7.5)TSGS(2.5) shows the highest FCP resistance as well as the highest fracture toughness (see Fig. 3).

at high stress intensity levels and is less potent in improving FCP resistance at near threshold regime. Indeed, Figure 4 shows that below a ΔK of 0.55 MPa $m^{0.5}$ (hereafter, referred to as the transition point ΔK_T), the rubber-modified epoxy polymer shows almost identical FCP resistance to that of unmodified epoxy. In contrast, the use of treated solid glass spheres (TSGSs) improves FCP resistance through the entire regime of fatigue crack growth when compared to that of neat epoxy. However, in the high crack growth rate regime (i.e., at growth rates exceeding 10^{-4} mm/cycle), solid glass spheres alone are not as efficient as rubber particles in improving FCP resistance. Interestingly, simultaneous use of both solid glass spheres and CTBN rubber results in further improvement in FCP resistance at both low and high ΔK levels at least for one of the hybrids; as can be seen from Figure 4, the R(7.5)TSGS(2.5) hybrid composite shows higher FCP resistance through the entire crack growth regime when compared to that of epoxy modified by either rubber or TSGS. Note that other hybrids also show higher FCP resistance almost up to a growth rate of 10^{-3} mm/cycle. This result suggests that a positive interaction occurs among the crack tip shielding mechanisms in the hybrid composites, thereby resulting in still higher FCP resistance. In order to more clearly show the occurrence of positive interactions in the R/TSGS hybrid composites, a plot of ΔK^*, the crack driving force (ΔK) required to produce a crack growth rate of 7.5×10^{-4} mm/cycle, versus the volume percent of both CTBN and TSGS was obtained from Figure 4 and is shown in Figure 5. The ΔK^* values for different materials were obtained by substituting 7.5×10^{-4} mm/cycle for da/dN in best-fit equations drawn through FCP data for each polymer system. Table III shows A and m values [the constants for the Paris–Erdogan equation[26] (Equation 3)] as well as ΔK^* values for the different compositions.

$$da/aN = A(\Delta K)^m \tag{3}$$

As can be seen from Figure 5, the FCP resistance of hybrid composites is greater than the FCP resistance expected from a simple rule of mixtures, thereby, confirming synergistic toughening in the hybrid system. The underlying reasons for FCP behavior of the materials studied are discussed in the following sections.

Crack Tip Shielding Mechanisms

The nature of the interactions among the crack tip shielding mechanisms causing synergistic toughening in the R/TSGS hybrid system was elucidated through study of the fatigue fracture surfaces and subsurfaces of the R(10), TSGS(10), and R(7.5)TSGS(2.5) (the composite with the highest crack growth resistance) materials. The corresponding SEM micrographs from the fatigue fracture surfaces of these materials obtained under secondary electron imaging conditions are presented in Figures 6 through 10. Further elucidation of the active shielding mechanisms was obtained through transmitted light optical microscopy (TOM) as shown in Figures 11 and 12. Observations of these composites will be discussed separately.

Table III Constants (A and m) of the Paris–Erdogan Power Law and ΔK Values at a Growth Rate of 7.5×10^{-4} mm/cycle for the Materials Studied

Composition	A	m	ΔK^a (MPa $m^{0.5}$)
Neat	1.19×10^{-3}	9.0	0.95
R(10)	1.80×10^{-4}	4.9	1.37
TSGS(10)	2.18×10^{-4}	8.3	1.16
R(2.5)TSGS(7.5)	1.10×10^{-4}	7.6	1.29
R(5)TSGS(5)	7.58×10^{-5}	6.9	1.39
R(7.5)TSGS(2.5)	4.11×10^{-5}	5.9	1.64
R(7.5)SGS(2.5)	5.69×10^{-5}	6.0	1.54

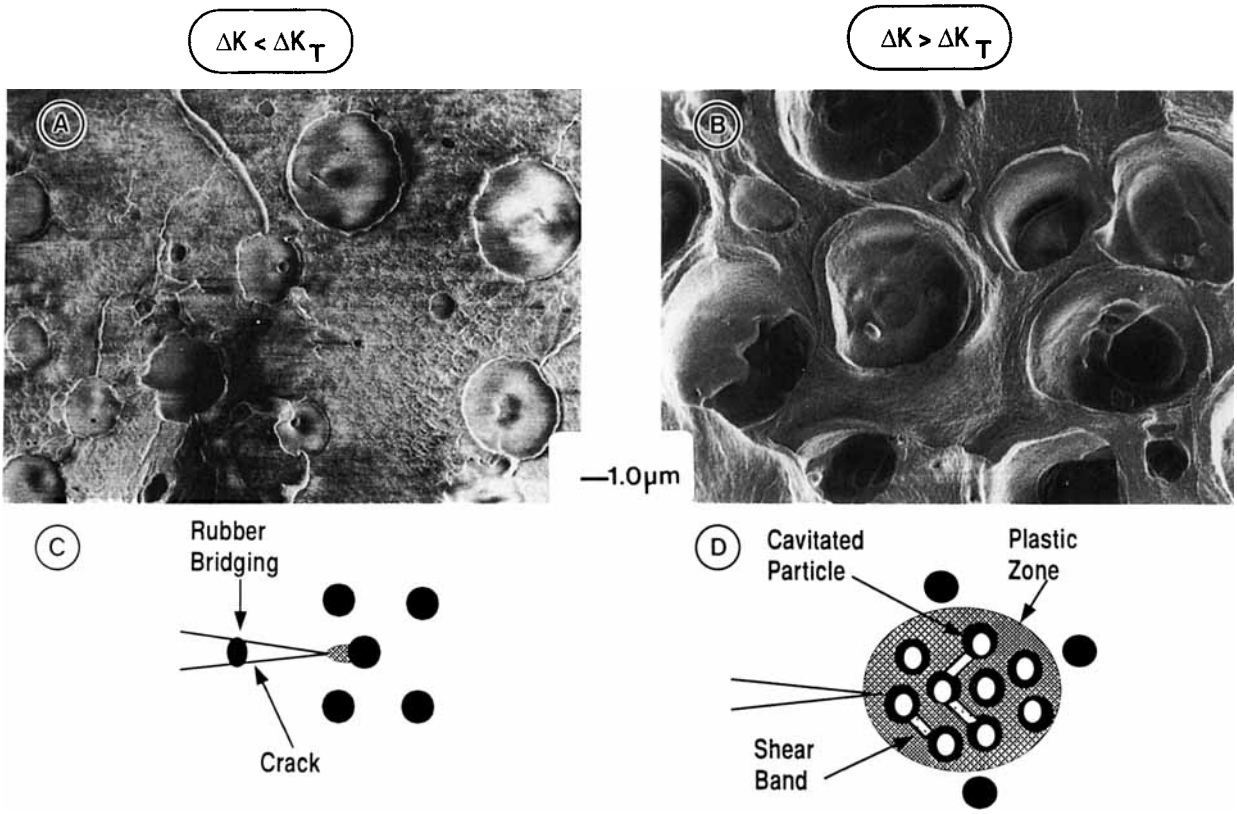

Figure 6 SEM micrographs showing the fatigue fracture surfaces of R(10) material; (a) at ΔK = 0.5 MPa $m^{0.5}$ (b) at ΔK = 2.5 MPa $m^{0.5}$. Note severe rubber cavitation and matrix dilation at high ΔK as opposed to low ΔK. Schematic drawings in (c) and (d) describe the crack tip plastic zone–particle interactions as related to micrographs (a) and (b), respectively. Arrow indicates the global direction of the FCP.[24]

Rubber-modified Epoxy

As already mentioned, a transition is observed in the FCP resistance of R(10) material at ΔK_T = 0.55 MPa $m^{0.5}$. Using Irwin's formula for the size of the plastic zone corresponding to plane strain conditions [Eq. (4)], it is found that the unique value of ΔK_T corresponds to the point where the plastic zone size, r_y, is on the order of the size of the rubber particles[24]

$$r_y = \frac{1}{6\pi}\left(\frac{K}{\sigma_y}\right)^2 \tag{4}$$

where r_y represents the radius of the plastic zone, and K and σ_y represent the maximum stress intensity at the transition point and the tensile yield strength of the neat epoxy, respectively. Such calculations reveal that the size of the plastic zone is about 3.5 μm at the empirically determined transition point (ΔK_T). Since the average size of the rubber particles is about 3 μm, it is reasonable to believe that these particles do not interact with the crack tip when ΔK is smaller than the ΔK_T. Alternatively, when the size of the plastic zone at the crack tip is large enough so that the rubber particles can be engulfed in the plastic zone and thus interact with the crack tip stress field (i.e., when $\Delta K > \Delta K_T$), the cavitation/shear yielding mechanisms become active (see Figs. 4 and 6). This result agrees well with the results by Pearson and Yee[9] on the effect of rubber particle size on toughening mechanisms in rubber-modified epoxy polymers. The results by these investigators show that, under monotonic loading conditions, when the size of the rubber particles is larger than the size of the formal plastic zone [given by Eq. (4)], rubber particles simply bridge the two crack surfaces and do not result in significant toughness improvement. In contrast, particles smaller than this size are embedded in the stress field of the crack tip, which then cavitate and promote shear yielding. The shear yielding of the surrounding matrix is a far more efficient toughening mechanism than bridging by rubber particles.

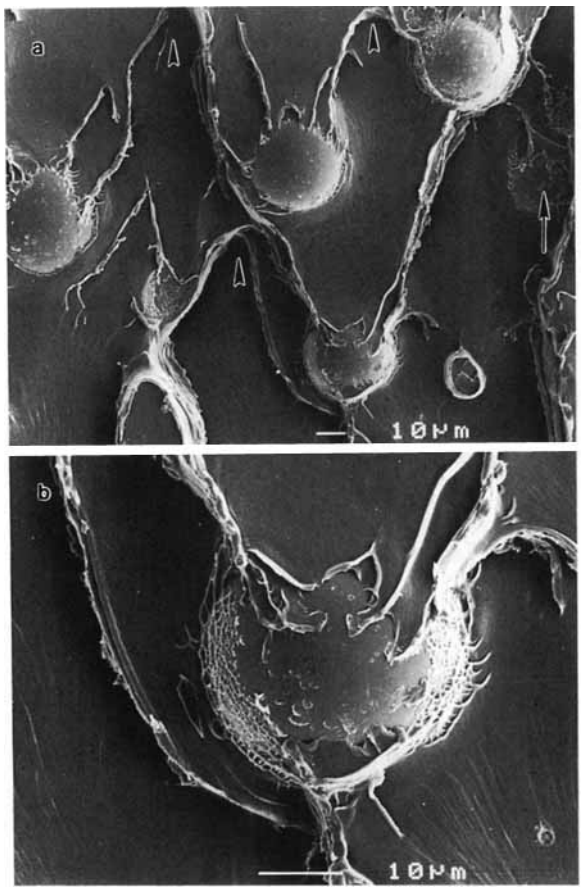

Figure 7 SEM micrographs at two different magnifications from the fatigue fracture surfaces of the TSGS(10) composites at ΔK = 0.6 MPa $m^{0.5}$. Arrow indicates the FCP direction. Small arrows in micrograph (a) indicate the crack bowing phenomenon between the glass spheres.

The transition phenomenon can also be documented by noting differences in the interaction between the plastic zone and the rubber particles, as revealed in SEM studies; it is expected that the operative shielding mechanisms would act differently at ΔK levels below and above ΔK_T. Therefore, the fatigue fracture surfaces of the rubber-modified epoxy polymer were examined at ΔK levels of 0.5 and 2.5 MPa $m^{0.5}$. The corresponding micrographs are shown in Figures 6(a) and 6(b), respectively. Figure 6(a) reveals the lack of rubber cavitation and matrix dilation when $\Delta K < \Delta K_T$, which can be attributed to the crack tip plastic zone size being less than the size of the rubber particles. The latter suggests that such particles should have acted as bridging agents. Indeed, features indicative of rubber bridging can be seen from Figure 6(a). However, rubber bridging does not result in improvement in FCP resistance [i.e., below ΔK_T, R(10) acts like neat epoxy] due to poor bridging efficiency of the rubber particles. On the other hand, from Figure 6(b), which corresponds to $\Delta K > \Delta K_T$, rubber cavitation and plastic dilation of the matrix around the cavitated rubber particles are evident. For a more detailed discussion on this issue, the reader is referred to a companion paper.[25]

Several crack tip shielding mechanisms for the rubber-modified epoxy, i.e., R(10), subjected to cyclic loading can be identified by carefully examining the SEM and TOM micrographs shown in Figures 6 and 11. These mechanisms include (a) rubber particles (engulfed in the process zone at the crack tip), which cavitate and enable the matrix around these cavities to dilate plastically, and (b) matrix ligaments between the cavities, which draw in plastically and give rise to high ridges seen around the cavitated

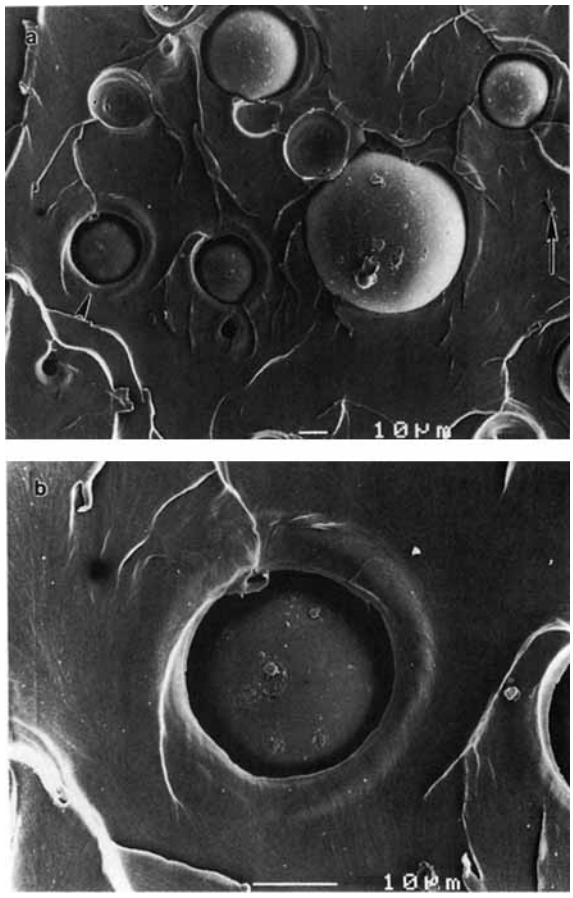

Figure 8 SEM micrographs at two different magnifications from the fatigue fracture surfaces of the TSGS(10) composites at ΔK = 1.5 MPa $m^{0.5}$. Arrow indicates the FCP direction. Compare this with the micrographs in Figure 7 and note that at a higher ΔK level smaller particles are debonded from the matrix.

rubber particles [Fig. 6(b)]. This latter feature has never been reported for the case of static fracture toughness testing of rubber-modified epoxies. Accordingly, it confirms the previous findings[19] that the failure micromechanisms and fracture surfaces generated by stable fatigue crack growth, even in a tension–tension mode, may reveal significantly different features from those generated under monotonic loading conditions. However, this feature is rather similar to dilatational bands that has been recently proposed by Lazzeri and Bucknall[27] for rubber-toughened polymers. The third operative mechanism involves heterogenous plastic deformation or shear bands that are formed between the rubber particles in the process zone of the crack tip (Fig. 11). The birefringent pattern seen in Figure 11(b) confirms that the dark region around the crack [Fig. 11(a)] is, indeed, a shear yielded zone.

SGS-modified Epoxy

Crack tip pinning by solid glass spheres is the primary shielding mechanism in TSGS(10) composite. Figures 7 and 8 show the fatigue fracture surfaces of the TSGS(10) composite for ΔK levels of 0.6 and 1.5 MPa $m^{0.5}$, respectively. The mechanism of crack tip pinning and subsequent crack bowing between the particles is clearly shown in Figure 7. Small arrows in this figure point to the crack bowing phenomenon between the glass spheres. Furthermore, as can be seen from this figure, no particle debonding is seen, as opposed to Figure 8 which corresponds to a ΔK of 1.5 MPa $m^{0.5}$. This suggests that at a ΔK of 0.6 MPa $m^{0.5}$, the glass particles are not engulfed within the crack tip stress field; therefore, the interface between the particles and the matrix remains intact at least until the crack front breaks away from the particles [i.e., see Fig. 7(b)]. Similar observations have been reported for fatigue of SiC–particulate metal matrix composites.[28,29] The intact interfaces along with high-strength particles, i.e., compared to the matrix strength, provide the proper conditions for the particles to pin the crack front.[12] Subsequently, the crack bows between these impenetrable particles [see arrows in Fig. 7(a)]. This process in turn results in a decrease in the crack driving force along the bowed segments and a corresponding increase in the crack driving force at the particle due to line tension effects.[12] In the present case, the bowing process is maintained until the interface between particle and matrix breaks down, whereupon crack advance resumes. Note that the solid glass spheres separate at the particle–matrix interface

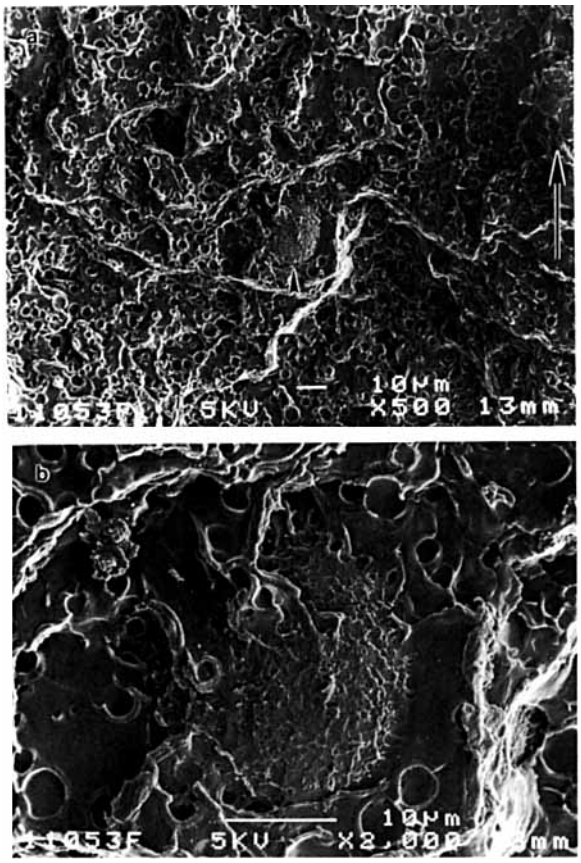

Figure 9 SEM micrographs showing the fatigue fracture surfaces of the R(7.5)TSGS(2.5) hybrid composite at two different magnifications at a ΔK level of 0.7 MPa $m^{0.5}$. Note rubber cavitation as well as the glass particle–matrix being intact. Arrow indicates the FCP direction.

rather than by fracture of the particles. Figure 13 shows a schematic drawing of slowing down of crack front advance by the pinning mechanism similar to what is seen from Figure 7(a). The importance of crack pinning in increasing FCP resistance has also been reported for several other brittle polymer matrix composites containing solid glass spheres.[30]

The fact that the solid glass particles are not engulfed in the crack tip stress field at low ΔK levels can be justified by using an argument similar to that for rubber particle–plastic zone interactions.[24,31] Therefore, by substituting 0.67 MPa $m^{0.5}$ for K [corresponding to ΔK = 0.6 MPa $m^{0.5}$ in Fig. 7(a)] and 71.2 MPa for the yield stress in Eq. (4), the plastic zone size is found to be approximately 5 μm; accordingly, the glass spheres will not influence deformation in the plastic zone ahead of the crack tip (the glass spheres average surface-to-surface spacing and average diameter being $\sim$ 37 and 49 μm, re-

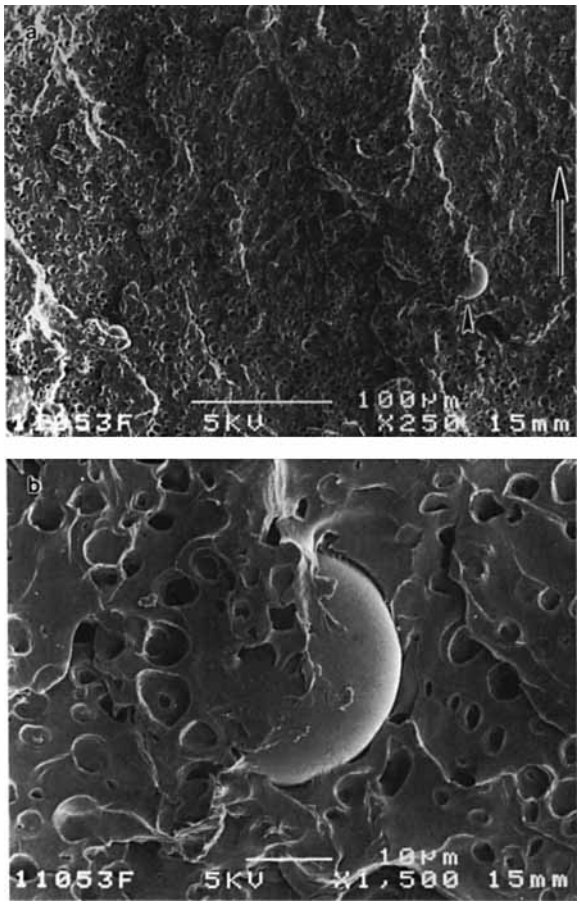

Figure 10 SEM micrographs showing the fatigue fracture surfaces of the R(7.5)TSGS(2.5) hybrid composite at two different magnifications at a ΔK level of 2.5 MPa $m^{0.5}$. Note rubber cavitation as well as the glass particle being covered by a layer of rubber and epoxy. Arrow indicates the FCP direction.

spectively). Although the matrix controls crack propagation at low ΔK levels, the surface roughness (i.e., the degree of crack deflection) is controlled by the reinforcement. Therefore, one may conclude that higher threshold values would be obtained if rod-shaped particles were used in place of spherical particles. The latter is in agreement with both experimental observations[28,32,33] and theoretical predictions.[34]

The effect of particle debonding and consequent enhanced shear yielding on the toughness of particulate-filled polymers has been discussed by Evans et al.[35] In contrast to low ΔK levels, the fatigue fracture surfaces corresponding to a ΔK of 1.5 MPa $m^{0.5}$ (Fig. 8) show that the smaller particles debond from the matrix. Glass particle debonding is then followed by matrix plastic dilation. Also, ridges can be seen around the debonded particles [Fig. 8(b)], which indicates that the matrix ligaments around the debonded particles have been drawn in plastically. The process of debonding and consequent plastic dilation is caused by the tensile radial stress component of the crack tip stress field.[36] Upon particle debonding, the triaxility at the crack tip is reduced and results in enhancement in shear yielding. This process shields the crack tip from the applied stresses, thereby improving the FCP resistance of the composite.

Another important feature of the micrographs shown in Figure 8 is the position of the crack plane with respect to the smaller particles (i.e., particles that have interacted with the crack tip plastic zone).

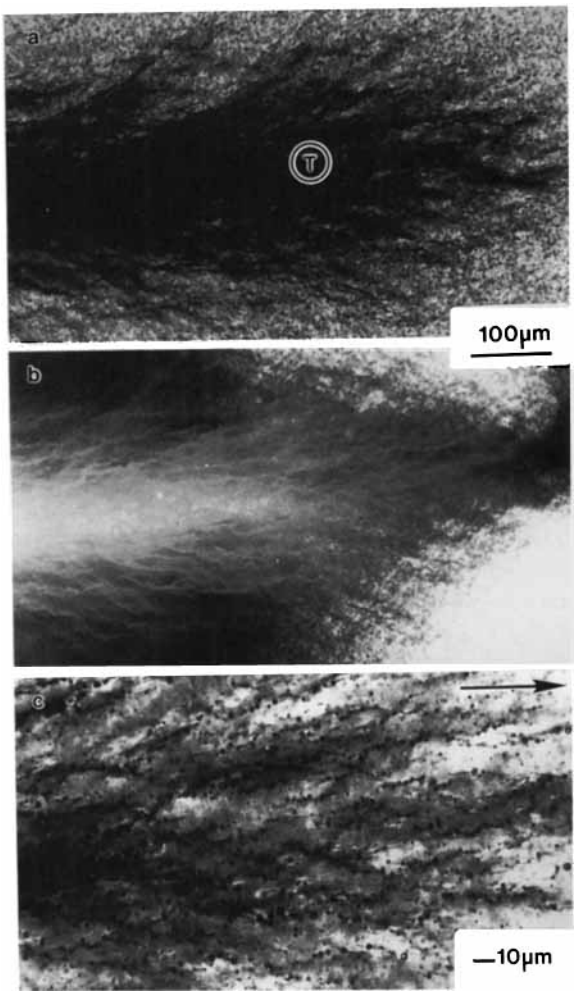

Figure 11 Optical micrographs from the subfatigue fracture surfaces illustrating shear yielding in R(10) material; (a) and (c) transmitted light and bright field (b) and crossed polars. Arrow indicates the FCP direction. Micrographs were taken at ΔK = 2.5 MPa $m^{0.5}$.[25]

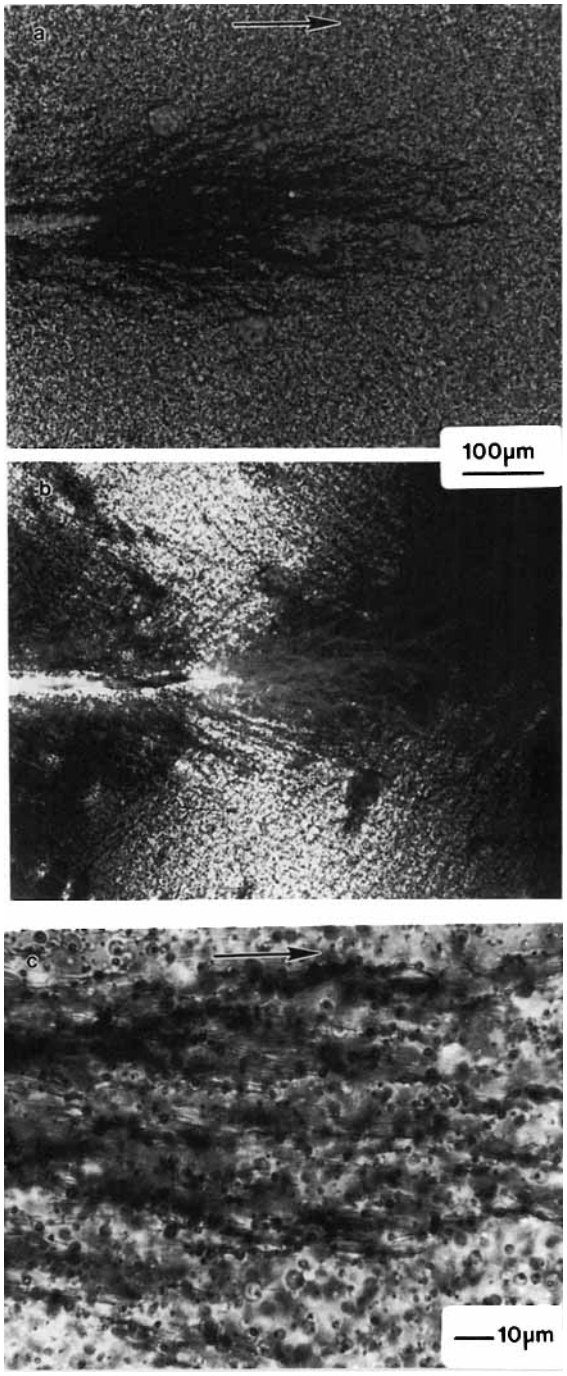

Figure 12 TOM micrographs showing the subfatigue fracture surfaces of the R(7.5)TSGS(2.5) hybrid composite at a ΔK level of 2.5 MPa $m^{0.5}$; (a) and (c) transmitted light and bright field and (b) crossed polars. Arrow indicates the FCP direction.

From these micrographs, it seems that the crack is attracted toward the pole of the smaller spheres. This in turn indicates that the position of maximum stress concentration is around the pole of the particles, which is consistent with the finite-element analysis by Guild and Young.[37] Figure 14 shows the result of the finite-element model by these investigators for an epoxy polymer filled with glass spheres. Note that both stress concentrations for the applied stress and for the radial stress are maximized at the pole of the sphere. Also, Figure 14 indicates that both applied and radial stresses are tensile at the pole and compressive at the equator.

Hybrid Epoxy Composite

Crack tip shielding mechanisms in R(7.5)TSGS(2.5) hybrid composite can be elucidated by studying SEM and TOM micrographs for this material as shown in Figures 9, 10, and 12. These micrographs which correspond to ΔK levels of 0.7 MPa $m^{0.5}$ (Fig. 9) and 2.5 MPa $m^{0.5}$ (Figs. 10 and 12) reveal that during cyclic loading several mechanisms are operative: (a) rubber particles interact with the crack tip stress field, cavitate, and reduce the triaxial stress in front of the crack; (b) as a result of the reduction in triaxial stress, shear bands form in the plastic zone in front of the crack (Fig. 12);[8,9] (c) shear banding of the matrix facilitates plastic void growth around the cavitated rubber particles;[38] and (d) the reduction in tensile triaxial stress resulting from rubber particle cavitation reduces the driving force for glass particle debonding from the matrix.

The interaction(s) among the crack tip shielding mechanisms, which has resulted in synergistic toughening in R(7.5)TSGS(2.5), can be identified by carefully comparing the fatigue fracture surfaces

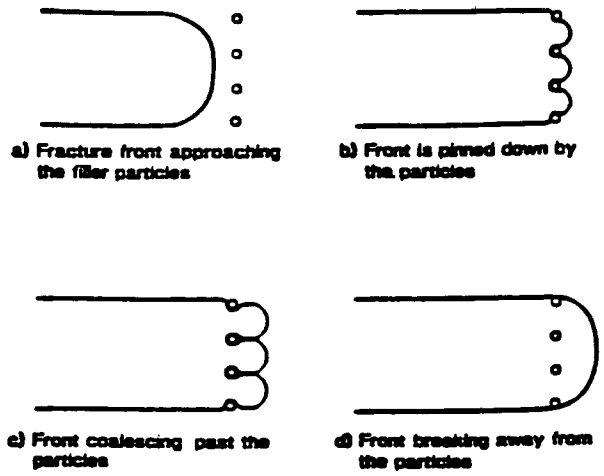

Figure 13 A schematic drawing showing the slowing down process of the crack front by pinning mechanism as illustrated in Figure 7(a).[29]

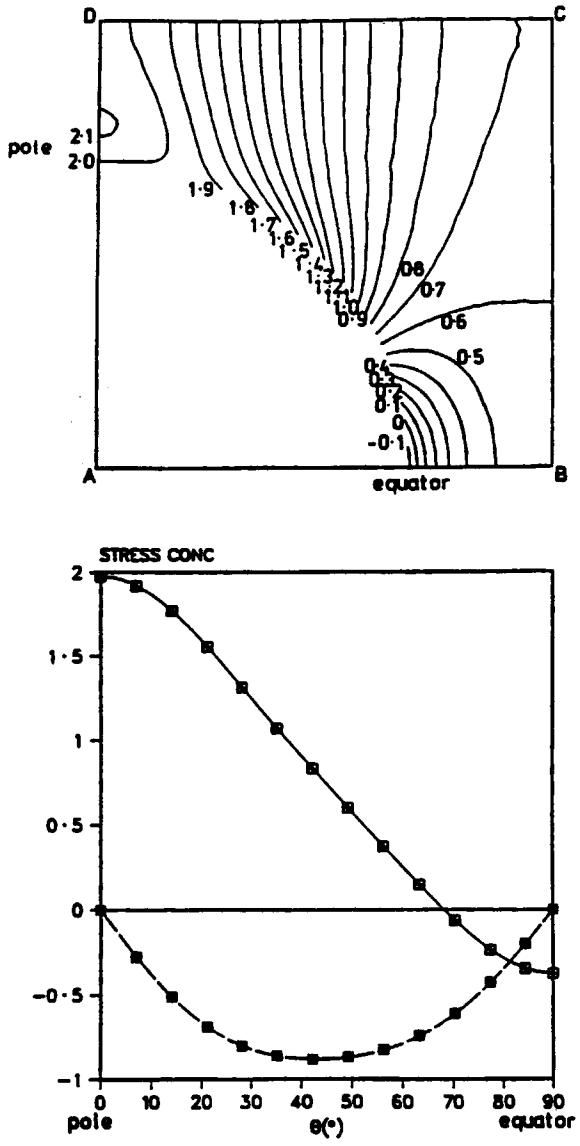

Figure 14 Finite-element results from Guild and Young[37] for a glass-filled (~20 vol % glass) epoxy with good adhesion. Note that both the applied stress and the radial tensile stresses are maximized at the pole of the spheres.

of this hybrid composite with those of the TSGS(10) composite [see Figs. 8(b) and 10(b)]. Figure 8(b) shows the fatigue fracture surface of TSGS(10) composite at a ΔK of 1.5 MPa $m^{0.5}$, whereas Figure 10(b) represents the fatigue fracture surface of the hybrid composite at a ΔK of 2.5 MPa $m^{0.5}$. As can be seen from Figure 10(b), the interface between the glass particles and the matrix in the hybrid composite is relatively intact as compared to the TSGS(10) composite, even though the glass particles in the hybrid composite are subjected to a larger applied stress field (i.e., K of 2.5 vs. 1.5 MPa $m^{0.5}$). Such behavior in the hybrid system is believed to originate from rubber particle cavitation. As was mentioned before, rubber cavitation results in a reduction in the hydrostatic component of the stresses around the glass particles. In other words, the driving force for glass particle debonding is reduced, following the cavitation of the rubber particles. Therefore, the interface between the glass particles and the matrix remains intact. This, in turn, increases the pinning/bridging efficiency of the glass particles in the hybrid system. The improved pinning/bridging efficiency of the glass particles and a change in the stress state caused by rubber cavitation are, therefore, believed to be the causes for synergistic behavior in the R(7.5)TSGS(2.5) hybrid composite.

The higher threshold stress intensity range factor (ΔK_{th}) for the hybrid composite when compared to that for TSGS(10) composite provides additional evidence for the positive interactions between the rubber particle cavitation/shear banding and the glass sphere pinning mechanisms. Indeed, it is sometimes assumed that crack propagation is related to the crack tip opening displacement.[39,40] This leads to a prediction in which the threshold stress intensity range factor (ΔK_{th}) is proportional to $(E\sigma_y)^{0.5}$, where E and σ_y represent the modulus of elasticity and the yield strength of the material, respectively. If this criterion is used, one would expect a higher ΔK_{th} for the TSGS(10) composite when compared to that for R(7.5)TSGS(2.5) hybrid composite since the TSGS(10) composite has both higher elastic modulus and yield stress when compared to its counterpart (see Table II). In contrast to the prediction, as can be seen from Figure 15, the hybrid composite shows higher FCP resistance near the threshold regime. It is believed that this behavior is caused by higher pinning/bridging efficiency of the glass particles and by a change in the stress state induced by rubber cavitation in the hybrid composite.

Role of Glass Particle–Matrix Interface

While some experimental results show that an improvement in the adhesion between solid glass particles and the matrix does not change the fracture toughness in glass-filled epoxy polymers,[5] other results[15,41] indicate an improvement in fracture toughness with increasing adhesion. As already mentioned, Kinloch et al.[15] claimed that improving the adhesion between glass beads and a rubber-modified epoxy matrix resulted in a synergistic in-

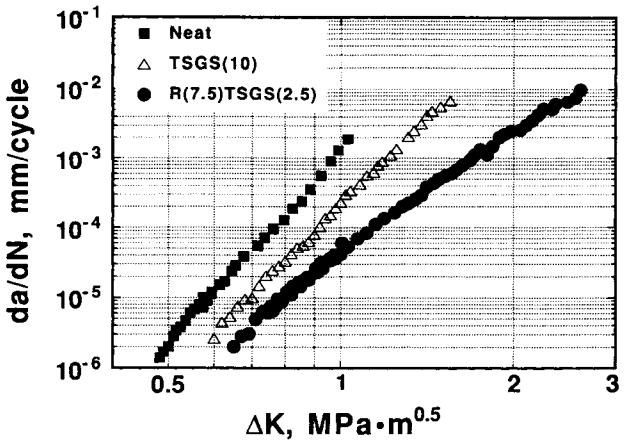

Figure 15 FCP data pairs for neat, TSGS(10), and R(7.5)TSGS(2.5) materials. Note that the hybrid composite shows higher FCP resistance at near threshold regime even though it has lower yield strength and lower Young's modulus compared to the other two materials (see Table II).

crease in the fracture toughness of their hybrid epoxy system due to an increase in pinning efficiency of the glass particles. In order to investigate the role of adhesion on the synergistic interactions under cyclic loading conditions, a hybrid epoxy with a formulation similar to the one with the highest FCP resistance was prepared, but the glass spheres were not given any coating, R(7.5)SGS(2.5), (SGS referring to solid glass spheres without any coating). The tensile properties, fracture toughness, and the FCP behavior of this material are shown in Table II and Figure 16. As can be seen from Table II and Figure 16, the surface treatment has almost no effect on the FCP resistance nor on the fracture toughness of the hybrid composite. These results are consistent with the SEM micrographs shown in Figure 10. As shown in Figure 10 and as previously discussed, glass particle debonding is suppressed in the presence of rubber particles. This was attributed to a reduction in the tensile triaxial stresses around the glass spheres upon rubber cavitation. This, in turn, may imply that the adhesion between glass particles and the matrix should not be important in the presence of rubber particles. The latter conclusion is consistent with the SEM micrographs shown in Figure 17. This figure shows the fatigue fracture surfaces of the hybrid composite with nontreated glass particles [i.e., R(7.5)SGS(2.5)] at a ΔK of 2.5 MPa $m^{0.5}$ and reveals no difference in the fracture surfaces of the treated and nontreated glass spheres. Therefore, it is reasonable to conclude that when rubber particles cavitate in the vicinity of the glass spheres, glass particle debonding from the matrix is suppressed, and thereby the interface between glass particles and the matrix remains intact, regardless of the nature of the interface.

CONCLUSIONS

Mixing various amounts of rubber and solid glass spheres into a ductile epoxy polymer, while keeping the total volume fraction of the modifiers constant at 10%, led to the development of a series of hybrid epoxy composites with improved FCP resistance. The FCP behavior as well as the crack tip shielding mechanisms operating under cyclic loading conditions were studied by careful examination of the fatigue fracture surfaces and the subfatigue fracture surfaces of fatigue samples. Furthermore the role of interfacial adhesion on synergistic interactions was considered. Based on the results obtained from this study, the following conclusions can be made:

1. Crack tip plastic zone–second phase particle interactions induce a transition in FCP behavior of rubber-modified epoxy polymer. Consequently, crack tip shielding mechanisms become active when the size of the plastic zone at the crack tip becomes large compared to the size of the rubber particles. That is, crack tip shielding mechanisms become active when the applied stress intensity exceeds the stress intensity range corresponding to the transition point (ΔK_T).

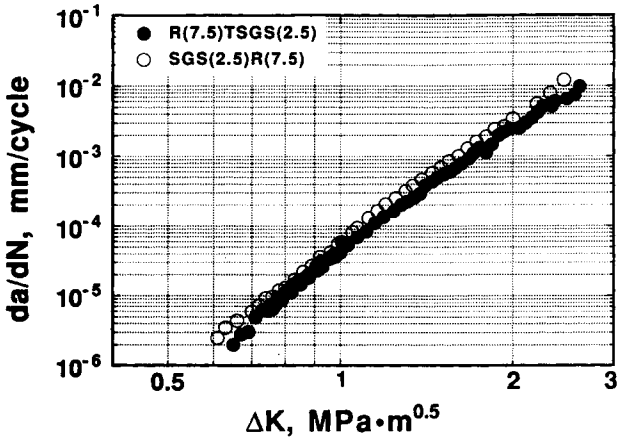

Figure 16 FCP data for hybrid composites with different interfacial properties. Note that the interfacial strength between glass particles and the matrix has very little effect on FCP data of hybrid composite.

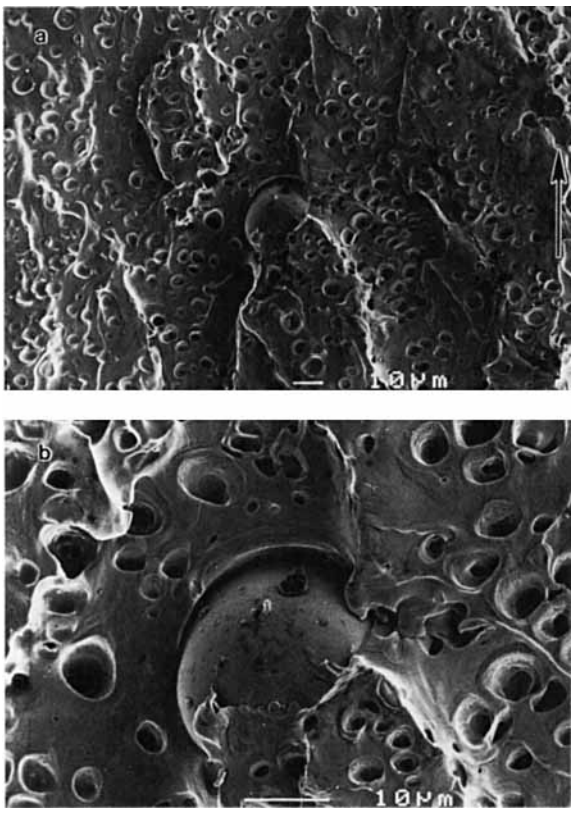

Figure 17 SEM micrographs showing the fatigue fracture surfaces of the R(7.5)SGS(2.5) hybrid composite at two different magnifications at a ΔK level of 2.5 MPa $m^{0.5}$. Compare these micrographs with those in Figure 10 and note that there is almost no difference in the fatigue fracture surfaces of treated and nontreated hybrid composites. Arrow indicates the global FCP direction.

2. While the FCP resistance of the epoxy polymer can be improved by the addition of rubber or solid glass spheres, the simultaneous use of rubber and solid glass spheres results in synergistic improvement in FCP resistance through the entire crack growth regime. This response is maximized for the case of the R(7.5)TSGS(2.5) hybrid epoxy composite.
3. Synergistic behavior observed in FCP resistance of hybrid composites is attributed to a change in the crack tip localized stress state, brought about by rubber cavitation, which also results in improved pinning/bridging efficiency of the glass spheres.
4. The interfacial adhesion between glass particles and the epoxy matrix has little effect on synergistic interactions in the hybrid systems studied. In fact, when rubber particles cavitate in the vicinity of the glass spheres, glass particle debonding from the matrix is suppressed, regardless of the nature of the interface.

The authors would like to thank the support provided by NSF-IUCRC for Polymer Interfaces Center at Lehigh University (NSF Grant No. ECD-9117064). Partial support by ACS-PRF Grant No. 25033-G7P is also appreciated.

REFERENCES

1. F. J. McGarry and A. M. Willner, *Org. Coat. Plast. Chem.*, **28,** 512 (1968).
2. A. J. Kinloch, S. J. Shaw, D. A. Tod, and D. L. Hunston, *Polymer,* **24,** 1355 (1983).
3. A. F. Yee and R. A. Pearson, *J. Mater. Sci.*, **21,** 2462 (1986).
4. J. Spanoudakis and R. J. Young, *J. Mater. Sci.*, **19,** 473 (1984).
5. A. C. Moloney, H. H. Kausch, T. Kaiser, and H. R. Beer, *J. Mater. Sci.*, **22,** 381 (1987).
6. Y. Huang and A. J. Kinloch, *J. Mater. Sci.*, **27,** 2763 (1992).
7. R. A. Pearson and A. F. Yee, *J. Mater. Sci.*, **21,** 2475 (1986).
8. A. G. Evans, Z. B. Ahmad, D. G. Gilbert, and P. W. R. Beamount, *Acta Metall.*, **34,** 79 (1986).
9. R. A. Pearson and A. F. Yee, *J. Mater. Sci.*, **26,** 3828 (1991).
10. X. C. Zhang, C. B. Bucknall, M. L. Orton, and G. V. Jackson, *9th Int. Conf. on Deformation, Yield and Fracture of Polymers,* Churchill College, Cambridge, UK, April 1994, p. 63/1.
11. F. F. Lange, *Phil. Mag.*, **22,** 983 (1971).
12. A. G. Evans, *Phil. Mag.*, **26,** 1327 (1972).
13. L. R. F. Rose, *Mech. Mater.*, **8,** 11 (1987).
14. B. Budiansky, J. C. Amazigo, and A. G. Evans, *J. Mech. Phys. Solids,* **36,** 167 (1988).
15. A. J. Kinloch, D. L. Maxwell, and R. J. Young, *J. Mater. Sci.*, **20,** 4169 (1985).
16. I. M. Low, S. Bandyopakhyay, and Y. W. Mai, *Polym. Inter.*, **27,** 131 (1992).
17. R. A. Pearson, A. K. Smith, and A. F. Yee, *2nd Inter. Conf. on Defor. & Frac. of Comp.,* The Plastics and Rubber Institute, London, 1993, p. 9-1.
18. J. C. Amazigo, and B. Budiansky, *J. Mech. Phys. Solids,* **36,** 581 (1988).
19. A. S. Holik, R. S. Kambour, S. Hobbs, and D. Fink, *Microstruct. Sci.*, **7,** 357 (1979).
20. J. A. Manson, R. W. Hertzberg, G. M. Connelly, and J. Hwang, *ACS Adv. Chem. Ser.*, **211,** 291 (1986).
21. J. Hwang, J. A. Manson, R. W. Hertzberg, G. A. Miller, and L. H. Sperling, *Polym. Eng. Sci.*, **29,** 1466 (1989).
22. J. Hwang, J. A. Manson, R. W. Hertzberg, G. A. Miller, and L. H. Sperling, *Polym. Eng. Sci.*, **29,** 1477 (1989).

23. J. Karger-Kocsis and K. Friedrich, *Comp. Sci. Tech.*, **48,** 263 (1993).
24. H. R. Azimi, R. A. Pearson, and R. W. Hertzberg, *J. Mater. Sci. Lett.*, **13,** 1460 (1994).
25. H. R. Azimi, R. A. Pearson, and R. W. Hertzberg, *J. Mater. Sci.*, to appear.
26. P. C. Paris and F. Erdogan, *J. Basic Eng. Trans. ASME, Series D,* **85,** 528 (1963).
27. A. Lazzeri and C. B. Bucknall, *J. Mater. Sci.*, **28,** 6799 (1993).
28. M. Gupta, K. Bowo, E. J. Lavernia, and J. C. Earthman, *Scripta Metal.*, **28,** 1053 (1993).
29. S. Kumai, K. Yoshida, Y. Higo, and S. Nunomura, *Int. J. Fatigue,* **14,** 105 (1992).
30. K. P. Gadkaree and G. Salee, *Polym. Compos.*, **4,** 19 (1983).
31. F. A. McClintock and G. R. Irwin, *ASTM STP 381,* 1965, p. 84.
32. H. R. Azimi, R. A. Pearson, and R. W. Hertzberg, *PMSE,* ACS, **70,** 250 (1994).
33. K. T. Faber and A. G. Evans, *Acta Metal.*, **31,** 577 (1983).
34. K. T. Faber and A. G. Evans, *Acta Metal.*, **31,** 565 (1983).
35. A. G. Evans, S. Williams, and P. W. R. Beaumont, *J. Mater. Sci.*, **20,** 3668 (1985).
36. M. E. J. Dekkers and D. Heikens, *J. Mater. Sci.*, **19,** 3271 (1984).
37. F. J. Guild and R. J. Young, *J. Mater. Sci.*, **24,** 298 (1989).
38. A. S. Argon, *Pure Appl. Chem.*, **43,** 247 (1975).
39. R. W. Hertzberg, in *Deformation and Fracture Mechanics of Engineering Materials,* 3rd ed., Wiley, New York, 1989.
40. C. J. Beevers, in *Fatigue Thresholds,* Warely, UK, 1981, p. 17.
41. N. Amdouni, H. Sautereau, J. F. Gerard, F. Fernagut, G. Coulon, and J. M. Lefebvre, *J. Mater. Sci.*, **25,** 1435 (1990).

Received November 1, 1994
Accepted February 1, 1995